JOURNAL OF COMPUTATIONAL PHYSICS 65, 273–291 (1986)

Some Tests of Precision for a Finite Element Model of Ocean Tides

C. LE PROVOST AND P. VINCENT

Institut de Mecanique de Grenoble, Grenoble, France

Received March 29, 1985; revised November 1, 1985

A finite element method is presented to solve the problem of ocean tides. A spectral (in time) model is implemented by deriving a second order partial differential equation from the classical shallow-water equations. The influence of several key factors on the precision of the method are investigated: density of triangles, degree of approximation and numerical integration, computer costs. Two analytical solutions are used as a reference: a damped Kelvin amphidrome in a channel of constant depth over a rotating earth, and a tidal wave propagating from the deep ocean over a continental plateau. The efficiency of the P2-Lagrange approximation is clearly demonstrated in terms of precision and computer costs. A criterion is established to guarantee a given precision, relating the basic grid size of the triangulation to be used to the typical wavelength of the tidal wave. An application of the model to the solution of a problem including a variable topography, rotation, nonlinear bottom friction and a tide-generating potential forcing is presented as a final complex test.

INTRODUCTION

During these past ten years, important progress has been done in ocean tide modelling, by improving the analytical formulations of the problem, and the numerical resolution of the corresponding equations over the whole real ocean (see Hendershott [8], Estes [4], Zahel [24], Accad and Pekeris [1], Schwiderski [22], Parke and Hendershott [18], Gotlib and Kagan [6], Parke [19]).

But the obtained solutions are not yet fully satisfactory. One of the main difficulties is the correct simulation of the energy dissipation over the shallow continental shelves, which needs fine spatial resolution over there. Up till now, only finite difference techniques have been used for practical computations, with regular spatial resolution, going up to $1^\circ \times 1^\circ$, or very recently with different nested discretizations refined in specific areas as done by Krohn [10]. However, in engineering applications for coastal dynamics, another approach using finite element techniques is under development, based on the pioneering attempts of Grotkop [5], Connor and Wang [3], and Taylor and Davis [23]. The interest in finite element methods is related to their potential flexibility in the representation of complex boundary geometry, and the prescription of arbitrary grid point locations, and in the use of higher order local interpolations. Two alternative representations of time domain are undertaken in that context: time stepping and spectral formulation. By far, the first one is the most commonly used because it applies not only for periodic phenomena but more generally to any arbitrary (meteorological) forcing function.

0021-9991/86 $3.00

However, a significant saving of computer time can be obtained for periodic phenomena, like tides, by seeking periodic solutions. That spectral finite element approach for tidal modelling has been formulated simultaneously by several authors: Kawahara and Hasegawa [9], Pearson and Winter [20], Le Provost and Poncet [12], and successfully applied for the solution of practical coastal tide problems by Le Provost, Rougier, and Poncet [14].

Such a method can be extended for ocean tide computations. It presents the interest of using simultaneously large meshes of several degrees over the ocean and local refinements down to some tens of kilometers over the continental margin and along the coastal boundaries. The aim of this paper is to present that formulation, to investigate the basic criteria for a precise resolution of the problem (density of triangles over the domain related to the wavelength of the tidal oscillation, degree of approximation and precision of numerical integration) by reference to analytical solutions established for some typical tests, and to illustrate the performance of the model on a schematic application.

1. The Analytical Formulation

1.1. *The Equations and Boundary Conditions*

On the basis of the depth integrated shallow water equations, assuming a multiperiodic solution, the presence of a dominant wave in the spectrum (e.g., the lunar M_2 constituent), and using a perturbation scheme to linearize the problem (with a particular emphasis on bottom friction), Le Provost *et al.* [14] have formulated pseudo nonlinear spectral equations for the different tidal constituents, in a spherical coordinate frame related to the earth:

$$\begin{aligned}
(j\omega + r)\,\mu + (r' - f)\,v + \frac{g}{a\cos\varphi}\frac{\partial}{\partial\lambda}\alpha &= F_\mu \\
(r'' + f)\,\mu + (j\omega + r''')\,v + \frac{g}{a}\frac{\partial}{\partial\varphi} &= F_v \\
j\omega\alpha + \frac{1}{a\cos\varphi}\left\{\frac{\partial}{\partial\lambda}(H\mu) + \frac{\partial}{\partial\varphi}(Hv\cos\varphi)\right\} &= F_\alpha
\end{aligned} \tag{1}$$

where (α, μ, v) are the complex amplitude of the sea surface elevation and the eastward and northward components of the velocity V for a given component of frequency ω:

* λ, φ, a are the longitude, latitude, and earth radius.
* H is the undisturbed depth of water, g the gravity.
* f is the Coriolis parameter: $f = 2\Omega\cos\varphi$, with Ω angular velocity of the earth rotation.
* r, r', r'', and r''' are the quasi-linearized coefficients for bottom friction, depending on λ, φ.

When the perturbation developments are limited to the second order of

approximation $A_j A_k$ (A_k being the characteristic amplitude of index k wave), the analytical expressions of these coefficients are the following: For the dominant wave (of index 1):

$$r = r''' = \frac{C}{H} R_1$$

$$r' = \frac{C}{H} \frac{R_1'}{\omega_1} \frac{\partial}{\partial t} \qquad \text{and} \qquad r'' = -r'$$

where R_1 and R_1' are expressed as the products of the characteristic amplitude A_1 of the wave by the modulus of the velocity at the location (λ, φ) and respectively two different terms depending on the amplitude and phase of the velocity (see [14]).

For the other waves of index k: $r = C(R_k + R_k')/H$,

$$r' = r'' = CR_k''/H \qquad \text{and} \qquad r''' = C(R_k - R_k')/H$$

where R_k, R_k', R_k'' are coefficients similar to R_1 and R_1' and only depend on the dominant solution (see [14]).

* F_μ, F_ν, F_α are the forcing terms, including the tide generating potential for the astronomical constituents, and second-order advective or frictional terms for the nonlinear harmonics and wave–wave interaction constituents. For the astronomical waves, these terms are of the following form:

$$F_\mu = \frac{g}{a \cos \varphi} \frac{\partial}{\partial \lambda} \left\{ (1 + k_2 - h_2) \frac{\pi_k}{g} + \iint_{\text{ocean}} (G\alpha \, d\lambda \, d\varphi \cos \varphi) \right\}$$

$$F_\nu = \frac{g}{a} \frac{\partial}{\partial \varphi} \left\{ (1 + k_2 - h_2) \frac{\pi_k}{g} + \iint_{\text{ocean}} (G\alpha \, d\lambda \, d\varphi \cos \varphi) \right\}$$

$$F_\alpha = 0.$$

π_k is the primary astronomical tide generating potential for the wave of index k. h_2 and k_2 are the classical Love numbers. $\iint_{\text{ocean}} G\alpha \cos \varphi \, d\lambda \, d\varphi$ is a Green integral which represents the loading effects of the tide, and which will not be taken into account in the following numerical tests.

For second-order nonlinear waves, these terms are dependent on the nature of these constituents. For instance, for the M_4 wave (of index 2 in the following) which is the first harmonic of the M_2 dominant wave, these terms, if limited to the second order are as follows:

$$F_{\mu_2} = -\frac{1}{a \cos \varphi} \left[\mu_1 \frac{\partial}{\partial \lambda} \mu_1 - \nu_1 \frac{\partial}{\partial \varphi} (\mu_1 \cos \varphi) \right]$$

$$F_{\nu_2} = -\frac{1}{a \cos \varphi} \left[\mu_1 \frac{\partial \mu_1}{\partial \lambda} + \nu_1 \frac{\partial \nu_1}{\partial \varphi} \cos \varphi + \mu_1^2 \sin \varphi \right]$$

$$F_{\alpha_2} = -\frac{1}{a \cos \varphi} \left[\frac{\partial}{\partial \lambda} (\alpha_1 \mu_1) + \frac{\partial}{\partial \varphi} (\alpha_1 \nu_1 \cos \varphi) \right].$$

Note. The spectral form of (1), although under a linear or quasi-linear aspect, is thus fully representative of the nonlinear tidal dynamics over oceanic and shallow water areas (to the order of approximation retained in the perturbation developments). Only lateral mixing is for the moment not included in this formulation.

The boundary conditions associated with system (1), over a domain $\mathscr{D}$ are:

$$\begin{aligned} &\mathbf{V}\cdot\mathbf{n}=0 \text{ along coastal boundaries} \\ &\alpha=\alpha_0 \text{ given along open ocean limits.} \end{aligned} \tag{2}$$

For practical numerical applications, the finite element analog of (1) can be obtained by a direct application of the Galerkin procedure. However, it has been shown by Lynch [16] that numerical solutions computed from this formulation are subject to node to node oscillations.

Following Le Provost and Poncet [13], an alternative is to eliminate the velocity from (1), leading to the second-order equation:

$$j\omega\cos\varphi\,\alpha+\frac{\partial}{\partial\lambda}\left(B\frac{1}{\cos\varphi}\frac{\partial\alpha}{\partial\lambda}-D\frac{\partial\alpha}{\partial\varphi}\right)+\frac{\partial}{\partial\varphi}\left(A\cos\varphi\frac{\partial\alpha}{\partial\varphi}-C\frac{\partial\alpha}{\partial\lambda}\right)=\mathscr{F} \tag{3}$$

where

$$\mathscr{F}=F_x\cos\varphi+\frac{a}{g}\left\{\frac{\partial}{\partial\lambda}(B\cdot F_\mu-D\cdot F_\nu)+\frac{\partial}{\partial\varphi}(A\cdot F_\nu-C\cdot F_\mu)\cos\varphi\right\}$$

and

$$\begin{aligned} A&=(j\omega+r)\,E^{-1}, \qquad B=(j\omega+r''')\,E^{-1}, \\ C&=(r''+f)\,E^{-1}, \qquad D=(r'-f)\,E^{-1}, \\ E&=a^2[\omega^2+f^2+f(r'-r'')+r'r''-rr'''-j\omega(r+r'')](gH)^{-1}. \end{aligned}$$

Equation (3) is called the "wave equation" by Lynch and Gray [15]. It is a second-order equation of the Helmholtz type relative to the complex unknown α. It has to be solved under limit conditions (2). If necessary, the velocity field can be obtained from the α solution and its first derivatives by the relations:

$$\begin{aligned} \mu&=\frac{a}{H}\left[B\left(\frac{1}{\cos\varphi}\frac{\partial}{\partial\lambda}\alpha-\frac{a}{g}F_\mu\right)-D\left(\frac{\partial}{\partial\varphi}\alpha-\frac{a}{g}F_\nu\right)\right] \\ \nu&=\frac{a}{H}\left[A\left(\frac{\partial}{\partial\varphi}\alpha-\frac{a}{g}F_\nu\right)-C\left(\frac{1}{\cos\varphi}\frac{\partial}{\partial\lambda}\alpha-\frac{a}{g}F_\mu\right)\right]. \end{aligned} \tag{4}$$

Lynch [15] has shown the effectiveness of that wave equation formulation in eliminating the node to node oscillations previously noticed when solving the problem through the primitive system (1).

1.2. *Variational Formulation*

Considering the Sobolev space $H^1(\mathscr{D})$ the complex-valued functions and the first derivatives of which are square integrable on the domain $\mathscr{D}$, we introduce a subspace of $H^1(\mathscr{D})$ defined by

$$W(\alpha_0) = \{\alpha \in H^1(\mathscr{D}): \alpha = \alpha_0 \text{ on the open boundary}\}$$

where α and α_0 are assumed to be complex-valued functions. $W(0)$ is the translated vectorial subspace from the affine one $W(\alpha_0)$, with the norm induced by the scalar product

$$\langle \alpha, \beta \rangle_{W(0)} = \int_{\mathscr{D}} \{\alpha\beta^* + \mathbf{grad}(\alpha) \cdot \mathbf{grad}(\beta^*)\}\, d\mathscr{D}$$

("*" denotes the complex-conjugate and $d\mathscr{D}$ an element of area of $\mathscr{D}$).

In order to obtain a variational formulation, the wave equation (3) can be integrated over the domain $\mathscr{D}$ with a testing function β in $W(0)$. Assuming that the boundaries are regular enough, the use of a Green–Riemann integral allows to take into account the boundary conditions (2) and write an integral equation leading to the following problem:

Find a function α in $W(\alpha_0)$, such that $L_1(\alpha, \beta) = F_1(\beta)$, $\forall \beta \in W(0)$, where

$$L_1(\alpha, \beta) = \int_{\mathscr{D}} \left\{ -j\omega \cos\varphi \alpha\beta^* + \frac{B}{\cos\varphi} \frac{\partial}{\partial\lambda} \alpha \cdot \frac{\partial}{\partial\lambda} \beta^* \right.$$
$$\left. - D \frac{\partial}{\partial\varphi} \alpha \frac{\partial}{\partial\lambda} \beta^* + A \cos\varphi \frac{\partial}{\partial\varphi} \alpha \frac{\partial}{\partial\varphi} \beta^* - C \frac{\partial}{\partial\lambda} \alpha \frac{\partial}{\partial\varphi} \beta^* \right\} d\mathscr{D}$$

$$F_1(\beta) = \int_{\mathscr{D}} \left\{ -F_\alpha \cos\varphi\, \beta^* + \frac{a}{g} \left[(BF_\nu - DF_\mu) \frac{\partial}{\partial\lambda} \beta^* \right.\right.$$
$$\left.\left. + (AF_\nu - CF_\mu) \cos\varphi \frac{\partial}{\partial\varphi} \beta^* \right] \right\} d\mathscr{D}.$$

A theorem of existence and uniqueness has been established for all the waves in the tidal spectrum, under some assumptions of smoothness and order of magnitude for the variable frictional coefficients, the depth, and the forcing terms [13].

The numerical resolution of the variational problem is realized by classical Lagrange finite element methods. An automatic finite element package is used for the following applications. It has been built by Poncet [21] and adapted to solve automatically the tidal problem.

2. Tests of Precision

The aim of the paper is to establish a set of basic criteria to ascertain precise resolution in practical applications. The philosophy, in the following, is to apply

our numerical model to the resolution of some schematic cases for which it is possible to find an exact solution. The main characteristics of the ocean tide problem we investigate in these tests are:

—its wave-like behavior,

—its large scale, planetary extension,

—the drastic variability of the bathymetry between the real ocean and adjacent seas.

Two analytical solutions have been built, for (1) a channel of constant depth in a rotating framework and (2) a nonrotating channel but including a continental plateau.

2.1. *The Kelvin Amphidrome Tests*

2.1.1. *The Analytical Solution*

The geometry of the problem is shown on Fig.1a. We consider a zonal channel limited by two open boundaries at longitudes λ_1 and λ_2, and two solid walls at latitudes φ_1 and φ_2; the channel has a constant depth and is rotating with the earth. A tidal forcing is specified at the open limits. A bottom friction damping linearly related to the velocity field is retained. Tidal potential forcing is ignored. When considering a channel with a small width ($b = a \cdot (\varphi_2 - \varphi_1)$) compared to the external radius of deformation given by $R_d = (1/f)(g \cdot H)^{1/2}$, it is justified to look for solutions with only zonal flows ($v = 0$). Moreover, the small extent of the domain allows us to neglect the terrestrial curvature and look for solutions of system (1)

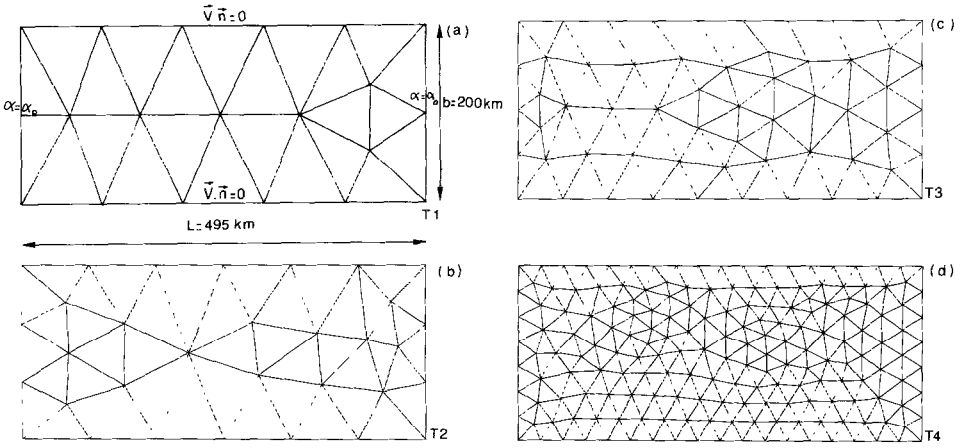

FIG. 1. (a) Kelvin amphidrome test domain: geometry and T_1 grid; (b) T_2; (c) T_3; (d) T_4.

written in a usual plane system of coordinates x and y. In that context, the general solution of (1) is

$$\alpha(x, y) = K \exp(y \cos\theta + x \sin\theta) \exp[j(y \sin\theta + x \cos\theta)] \tag{6}$$

$$\mu(x, y) = -\left(\frac{g}{k_0 H}\right)^{1/2} K \exp(j\theta)\, \alpha(x, y) \tag{6a}$$

with

$$\operatorname{tg}(2\theta) = \frac{r}{\omega} \qquad \text{and} \qquad k_0 = \left(1 + \frac{r^2}{\omega^2}\right)^{1/2}$$

$$X = x\omega\left(\frac{k_0}{gH}\right)^{1/2} \qquad \text{and} \qquad Y = yf\left(\frac{1}{gHk_0}\right)^{1/2}$$

K is a constant.

It represents a damped version of the classical Kelvin amphidrome valid for waves in narrow frictionless rotating channels [11]. One visualization is given on Fig. 2, for the following parameters: $L = 495$ km, $b = 200$ km, $H = 50$ m, $\omega = 1.4\ 10^{-4}\ s^{-1}$, $r = r''' = 3.12\ 10^{-5} s^{-1}$, $r' = r'' = 0\ s^{-1}$ and $K = 3$ m.

The sea surface elevations are decreasing down to zero at a point called "amphidromic point" around which the cophase lines are rotating.

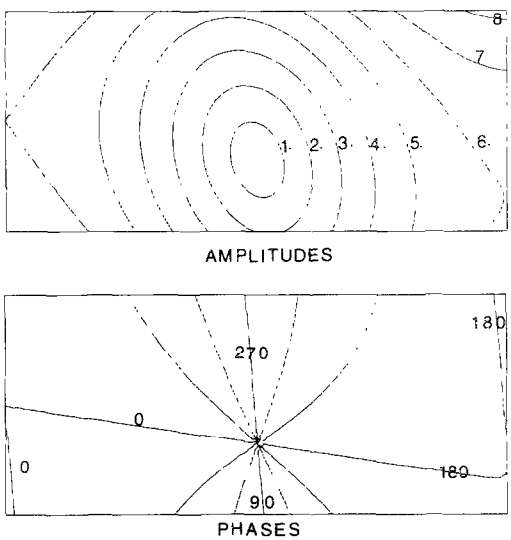

FIG. 2. Analytical solution for the damped Kelvin amphidrome (amplitudes of α in m, and phases in degrees).

2.1.2. *The Numerical Results*

The preceding result has been computed numerically with the finite element model presented in Section 1. The boundary conditions are taken from the analytical solution (Eq. (6) and (6a)) along the two meridional openings. In order to investigate the factors controlling the quality of the numerical calculations, several simulations have been done under different conditions. We have tested:

—the size of the triangles,

—the degree of the basic polynomials approximating the solution over each triangle.

—the degree of approximation of numerical integration (all the numerical computations are made with Hammer's formulas [7])

In order to rationalize the comparison between the analytical and the numerical solutions, an error norm has been computed over all the mesh points:

$$\varepsilon^2 = \sum (\text{sol.}_{\text{num}} - \text{sol.}_{\text{ex}})^2 \Big/ \sum \text{sol.}_{\text{ex}}^2$$

where sol._{num} denotes the finite element solution and sol._{ex} the exact one.

The standard deviations are displayed on Fig. 3 for the amplitudes of the sea-surface elevation (Fig. 3a) and the velocity (Fig. 3b). These diagrams illustrate the degree of precision which can be reached with a given density of triangles over the integrated physical domain.

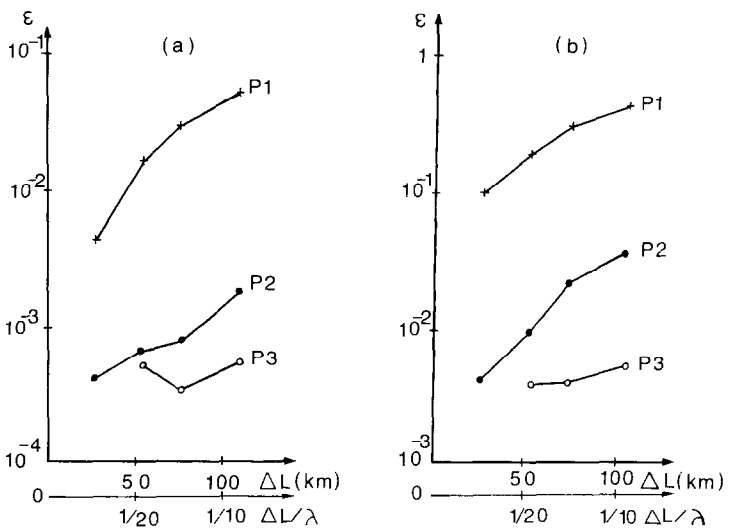

FIG. 3. Precision of the computed solutions: $\varepsilon^2 = \sum (\text{sol.}_{\text{num}} - \text{sol}_{\text{ex}})^2 / \sum \text{sol.}_{\text{ex}}^2$ (the ε-scale is logarithmic): (a) sea-level elevations; (b) modulus of μ-solution.

a. The different meshes. Four approximately regular grids have been used. They are presented on Figs. 1a, b, c, d. The typical mesh size vary from 1/10th to 1/40th of the wavelength of the studied phenomenon (defined as $\Lambda = 2\pi\omega^{-1}(gH)^{1/2}$):

—T_1: 22 triangles (maximum mesh size $\Delta L_{\max} = \Lambda/10$)

—T_2: 44 triangles ($\Delta L_{\max} = \Lambda/13$)

—T_3: 90 triangles ($\Delta L_{\max} = \Lambda/20$)

—T_4: 316 triangles ($\Delta L_{\max} = \Lambda/40$).

Figures 3a and b show that the precision of the solution is improved by a factor of 10 when increasing the space resolution from $\Lambda/10$ to $\Lambda/40$.

b. Influence of the degree of the basic polynomials. The three first elements of the Nicholaides family (P_1, P_2, P_3-Lagrange elements [17]) have been tested. In agreement with the theory, for a given triangulation, the solution is greatly improved by using higher order elements.

For the sea-surface evaluations, the precision of the solution is increased by a factor of 10 to 25 when using P_2 approximation instead of P_1; the gain is only of 3 or even less when going from P_2 to P_3.

For the velocities, which are derived from the α-solution through Eqs. (4), the precision is even more dependent of the choice of the basic polynomials. With P_1 approximation, the velocity-solutions are constant on each triangle, and it can be seen in Fig. 3b that the precision of the solutions is bad, even when refining the mesh down to $\Lambda/40$, and that precision is greatly improved by increasing the degree of approximation:

—by a factor 10 to 25 for P_2 instead of P_1,

—by a factor 2 to 8 for P_3 instead of P_2.

One should notice a phenomenon of "super-precision" for the currents at the center of gravity of each triangle, clearly established by a careful comparison between the results of computations and the analytical solution.

It must be noticed also, on Fig. 3, a surprising feature for the precision of the μ-solution with a P_3 approximation. We can observe on the lower curve of Fig. 3a an increase in the sea level error as the resolution increases.

c. Influence of numerical integration. An exact integration in $L_1(\alpha, \beta)$—see Eq. (5)—requires formulas of order $2k+1$ because of the term $\int_{\mathcal{D}} -j\omega \cos\varphi\, \alpha\beta^*\, d\mathcal{D}$, if the polynomial approximation of α is taken in P. For the other terms, a formula of order $2k-1$ is sufficient when the depth H and the frictional coefficients are constant, which is the case in that test. To estimate the influence of numerical integration, we have tested the following formulas:

—for a P_1 approximation of α: integration of order 1 and 3, respectively exact for polynomials in P_0 and P_2.

—for a P_2 approximation of α: integration of order 3 and 5, respectively exact in P_2 and P_4.

—for a P_3 approximation of α: integration of order 5 and 7, respectively exact in P_4 and P_6.

The results are presented in Figs. 4a and b, displayed in terms of computer cost (in anticipation of the analysis of the following paragraph). It can be observed that the precision gain is not very important when using a $2k+1$ order integration formula for P_1 and P_2 approximations. On the contrary, for a P_3 approximation, a noticeable difference can be pointed out between integrations of order 5 and 7, in favour of the latter. As we will conclude in the following that P_2 approximation is the most convenient for practical applications, a numerical integration exact for polynomials in P_{2k-1} appears to be sufficient for our purpose.

d. The computer costs. Figures 4a and b sum up the cost of the numerical experiments carried out in the Kelvin amphidrome test. Globally, the dependence between the cost, the number of triangles, and the order of approximation are classical:

—for a given cost, a better numerical solution is obtained when using higher order approximation.

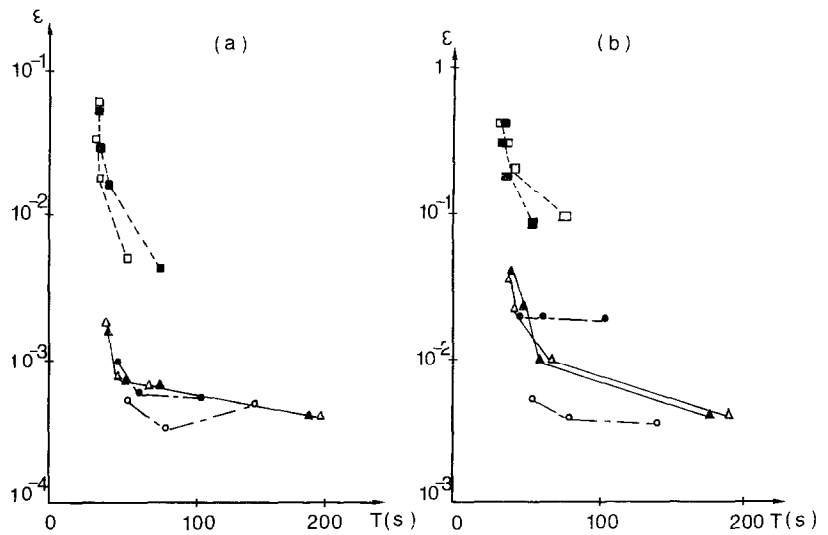

FIG. 4. Dependence precision-CPU time (T in s) (the computations were run on an HB68 computer): (a) sea-level elevations; (b) modulus of μ-solution. □: P_1-approximation, integration of order 1; ■: P_1-approximation, integration of order 3; ▲: P_2-approximation, integration of order 3; △: P_2-approximation, integration of order 5; ●: P_3-approximation, integration of order 5; ○: P_3-approximation, integration of order 7.

—the precision is greatly improved by refining the mesh, but only to a certain extent; for P_2-approximation, no significant gain is obtained when using T_3-triangulation instead of T_3. This is even more important for P_3-approximation.

The two diagrams lead to the conclusion that P_3-approximation is the most appropriate. However, this implies, for reasonable computer cost, the use of a limited number of triangles, which may be acceptable for the present case with a very regular geometry, but is totally inadequate for realistic domains with complex coastlines. For the same cost, quite the same precision can be achieved with P_2-elements, but with a higher spatial resolution for the triangulation. Moreover, for any type of approximation in P_k and a given triangulation, we have already noticed that no significant difference exists between $2k-1$ and $2k+1$ order integration formula, except when k is 3.

Consequently, it appears that the investigated test problem can be precisely and economically well solved with a P_2-approximation and a 3rd order integration formula.

e. Note about theoretical error estimations. Let us denote $\mathscr{H}^m$ the Sobolev space of order m for complex valued functions, and $\mathscr{L}^2$ the space of complex-valued fonctions the real part and the imaginary part of which are square integrable.

If we try to calculate the estimation error given by Arcangeli and Gout [2], we must evaluate $|\alpha|_{\mathscr{H}^2}$ and $|\alpha|_{\mathscr{H}^3}$ which are present in the following inequalities (see [21] for their calculus):

$$|\alpha - \alpha_{\text{num}}|_{\mathscr{L}^2} < 3d^2 |\alpha|_{\mathscr{H}^2} \qquad \text{for a } P_1\text{-approximation of } \alpha.$$

$$|\alpha - \alpha_{\text{num}}|_{\mathscr{L}^2} < d^3 |\alpha|_{\mathscr{H}^3} \qquad \text{for a } P_2\text{-approximation of } \alpha.$$

(d is the largest side of the triangles).

Computations of $|\alpha|_{\mathscr{H}^2}$ and $|\alpha|_{\mathscr{H}^3}$ can be carried out in terms of $|\alpha|_{\mathscr{L}^2}$ and we finally obtain estimations for the relative error in terms of $\mathscr{L}^2$-norm:

$$\frac{|\alpha - \alpha_{\text{num}}|_{\mathscr{L}^2}}{|\alpha|_{\mathscr{L}^2}} < 2.10^{-10} d^2 \qquad (P_1\text{-approximation})$$

$$\frac{|\alpha - \alpha_{\text{num}}|_{\mathscr{L}^2}}{|\alpha|_{\mathscr{L}^2}} < 4.10^{-16} d^3 \qquad (P_2\text{-approximation}).$$

For instance, when d takes the value 100 km, the relative errors in $\mathscr{L}^2$-norm are respectively 200% for a P_1-approximation and 40% for a P_2-approximation. These results prove that the error estimations only give orders of magnitude for the solutions, but fortunately are not realistic enough.

2.1.3. *Conclusion*

In order to obtain a satisfactory representation of the sea-level elevation and the velocity field, the use of the second element in the Nicholaides family with a reasonably refined mesh seems to be quite sufficient. Figure 3 suggests a criteria in

order to obtain a given precision for the α-solution, in terms of a fraction of the wavelength. An approximate precision of 10^{-2} for the velocity and 10^{-3} for the elevation in the ε-sense can be reached when choosing a maximum basic size of about $\Lambda/15$ for the triangles. In addition, this corresponds to the optimal level, from the economic point of view.

It is important to have in mind, however, that the problem solved for this test involves constant frictional coefficients which is not the case for real applications, especially when the domain includes shallow water areas. The preceding conclusion cannot consequently be definitely generalized to practical problems.

2.2. *The Continental Shelf Test*

2.2.1. *The Exact Solution*

The ocean tide problem includes the propagation of the tidal waves from the deep ocean (4000 m) to the shallow continental basins (less than 200 m). From the conclusions of the preceding chapter, a strategy can be adapted with our finite element model to fit the density of the triangulation to the resolution required for an expected precision, in relation with the depth over the different areas investigated. An exact solution has been built for the schematic case depicted in Fig. 5: the investigated domain includes a 4000 m deep flat bottom ocean, connected by a steep continental margin to a shallow basin gently sloping from 200 m to 10 m, and closed by a vertical wall at its end. The ocean tide is induced in that channel by the ocean side open boundary. The earth rotation and the bottom damping are ignored in that test case.

An exact solution can be calculated by solving the second-order partial differential equation (3) in the three subdomains S_1, S_2, S_3 characterized by their depth

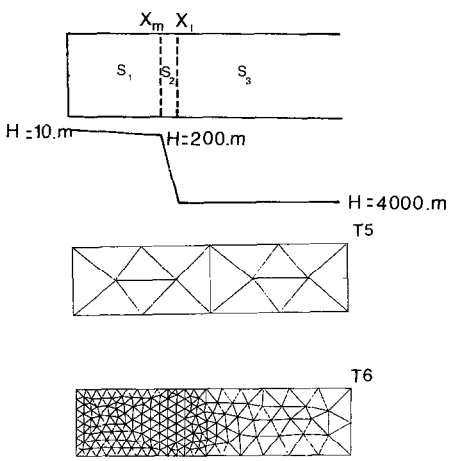

FIG. 5. Depth profile for the shelf experiment. Triangulations T_5 and T_6.

profile. The solution is completely determined by prescribing continuity conditions for α and μ at points X_m and X_I, a Dirichlet condition for α at the open boundary and a no flow condition at the wall. This solution is displayed in Fig. 6 in full line for an incident wave of 1 m in amplitude, propagating in a channel 890 km long, situated at the equator.

2.2.2. *The Numerical Results*

The numerical solutions desplayed in Fig. 6 have been computed under different conditions:

—With a uniform space resolution of 2° everywhere (T_5). In such a case, the mean value of the largest side of the triangles is about $A/40$ for the oceanic part of the domain but approximately $A/10$ when H is 200 m and $A/2$ when H is 10 m, which is too coarse over the shelf. Such a mesh size is commonly used in global ocean tide numerical modelling.

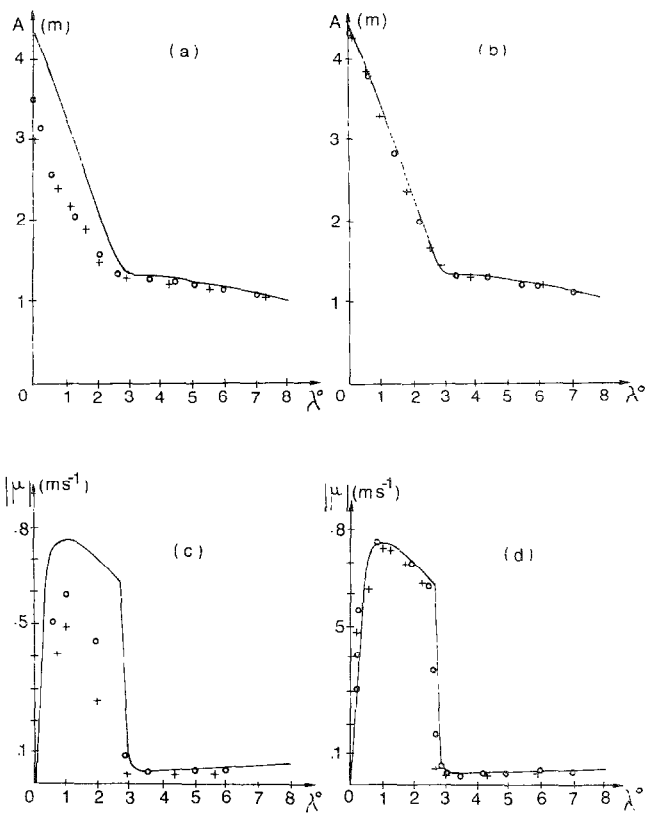

FIG. 6. Comparison of the numerical solutions (—, analytical; +, P_1-approximation; ○, P_2-approximation): (a) T_5-grid, sea-surface elevations (in m); (b) same as 6a, except for T_6; (c) T_5-grid, μ-velocity solutions (in $m \cdot s^{-1}$); (d) same as 6c, except for T_6

—With an adapted mesh on the shallow area based on the $\Lambda/15$ criterion with P_2-polynomials derived from Section 2.1.3 (T_6). This leads to typical mesh size of 0.3 degrees for this part of the domain.

—With first-order P_1 and second-order P_2 approximations. The results are plotted in Figs. 6a, b for the sea-surface elevations and 6c, d for the velocity field.

a. Results for the amplitudes. As expected from Section 2.1, the numerical solutions are all correct over the ocean; a small discrepancy can be observed however for the uniform coarse grid computations, of the order of 2 cm when approaching the continental slope. Over the continental shelf, the computed solution is far from the exact one for insufficient spatial resolution, even when using P_2 polynomials (see Fig. 6a). On the contrary, the solutions are excellent with a reasonable discretization (see Fig. 6b): the numerical solutions match the exact one everywhere in the ocean, the continental margin and the shallow water area.

b. Results for the currents. For the coarse grid, both approximation P_1 and P_2 do not give satisfying results. The amplitude of the velocity is too small and very far from the exact one. (The phases are not represented here, but it must be noticed that there is no problem to reproduce the exact phase solution for α and μ)

For the adapted mesh, results are very good for the P_2 approximation (see Fig. 6d). The maximum amplitude of the analytical solution is reached by the numerical one, which was clearly not the case when computing with the coarse grid. The P_1 solution gives currents which are not very different from the exact ones but the use of that first-order approximation has the drawback to supply constant currents on the triangles, which makes a good representation over the shelf difficult. Very good confidence can thus be placed in the numerical solutions computed with the present model under reasonable conditions.

3. Intercomparison for a Complex Exercise

The preceding tests based on analytical solutions do not allow to include other important ingredients of the problem of ocean tides. In the following, a more complex schematic exercise is presented including:

—a variable topography and earth rotation,

—a tide generating force,

—nonlinear shallow water bottom friction damping.

Evidently, it is not possible to obtain an analytical solution for that complex case. But a reference solution can be expected from a computation with P_2 polynomials and adequate resolution. And the aim of this section is to characterize the magnitude of the errors resulting from some drastic violations of the elementary rules pointed out in Section 2.1.3.

3.1. *Parameters of the Numerical Experiments—Grid Domains*

In that test, we consider a channel 3500 km long and 700 km wide, situated at a mean northern latitude of 50 degrees. This domain is taken on the earth and will always be displayed, in the following, in a horizontal and orthogonal system of spherical coordinates with longitude as abcissa and latitude as ordinate. The depth

westward shelf are included, each of them extending 300 km and gently sloping from 10 to 200 m.

Three different grids are built to solve the problem. The first one T_7 (see Fig. 7b) is very coarse, with a maximum step size of approximately 1/15th of the tidal wavelength for an ocean of 4000 m depth. This leads, for this regular coarse grid, to an approximate 7° mesh size.

The second grid, called T_8 (see Fig. 7c), is a regular grid with a uniform 2°-mesh as for the preceding shelf test, which is a typical discretization of the ocean used for global ocean tides modelling.

The third grid, called T_9 (see Fig. 7d), is built by application of the criterion derived from the conclusion of the Kelvin amphidrome test. Its mean mesh size is about 1/13th to 1/14th of the wavelength over the whole domain, even on the continental shelves.

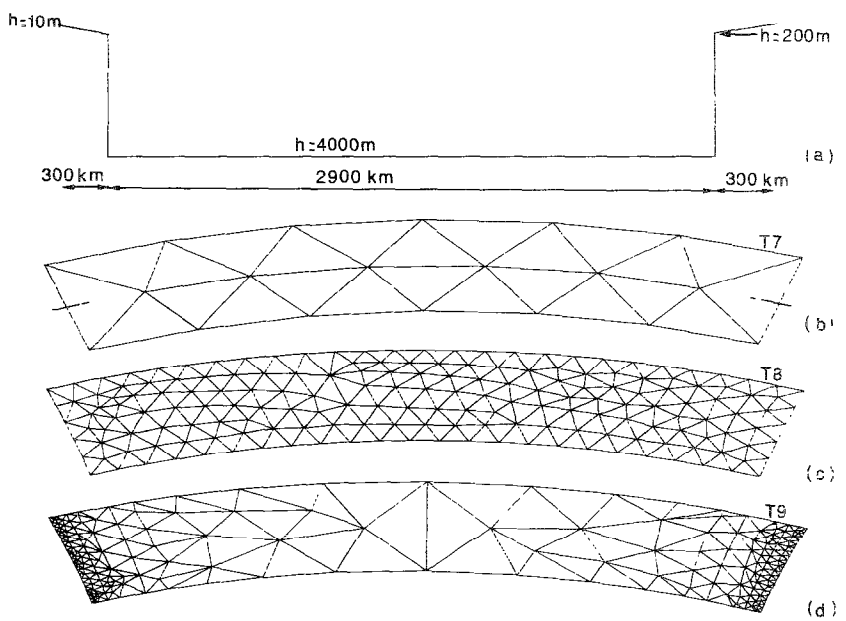

FIG. 7. (a) Depth profile for the complex exercise; (b) T_7-grid ($\Delta L_{max} = 7$ degrees); (c) T_8-grid ($\Delta L_{max} = 2$ degrees); (d) T_9-grid ($\Delta L_{max} = 1/14$th of the tidal wavelength everywhere).

P_1 and P_2 approximations are used to compute the solutions with our finite element model. The non-linearity due to the quasi-linearization of the quadratic law of bottom friction is resolved through an iterative process described in [13, 14].

3.2. *Results*

3.2.1. *General Features of the Solution*

We can legitimately consider that the solution computed with T_9-grid and P_2-elements is the most precise one, and we will use it as a reference in the following; hereafter, this solution is referenced as "*S*." This solution is displayed on Figures 8a, b. The decrease of the sea-surface elevation down to zero and the rotation of the cophase lines around the same point show the existence of an amphidrome. In the deep ocean, the amplitude of the *S*-solution increases up to 1.20 m, with a uniform spacing of the corange lines. On the continental shelves, the sea-surface elevations are enhanced up to 3.30 m.

3.3.2. *Comparison between P_1 and P_2 Approximations*

We do not present illustrations for the set of P_1-solutions because of lack of space. Let us comment however on the main conclusions of that comparison. As expected, the three P_1 solutions are all far from *S*. As a general rule, we observe, for each grid, an increase of 20 to 30% for the sea-surface elevation when using P_2 polynomials instead of P_1. For the "T_9–P_1" experiment, the maximum amplitude obtained for the α-solution is about 2.40 m instead of 3.30 m for *S*.

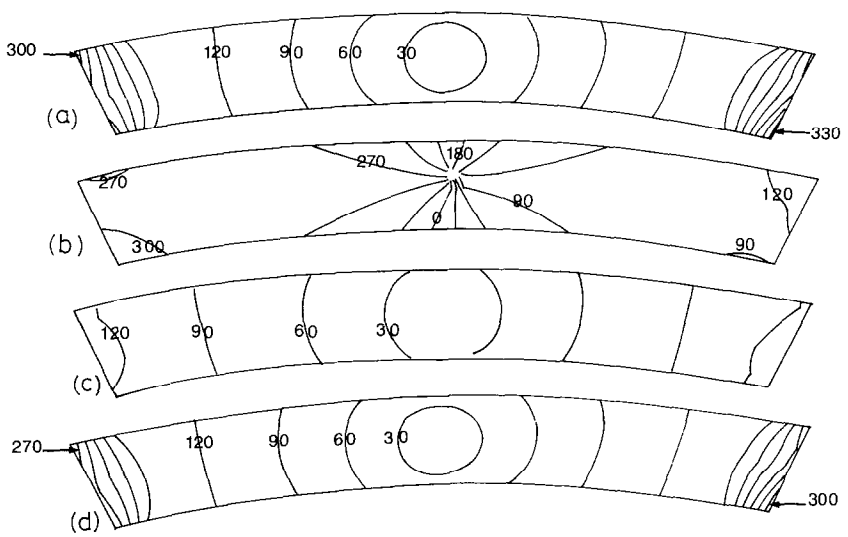

FIG. 8. (a) *S*-solution (T_9–P_2), amplitudes of the sea-surface elevations (in cm); (b) *S*-solution, phases distribution in degrees; (c) "T_7–P_2" solution, amplitudes of α (in cm); (d) "T_8–P_2" solution, amplitudes of α (in cm).

We know, from [13 and 14], that the present problem needs a correct resolution of the velocity field because of the nonlinear damping characteristics over the shelf. The present problem is much more difficult than the shelf one of Section 2.2, where the flow was cylindrical; here, the velocity field is bidimensional because of the presence of the earth rotation, and correct velocity solutions cannot be obtained with a P_1 approximation, unless a very fine grid is used everywhere. Consequently, from that comparison it is clear that at least P_2 polynomials are necessary to solve precisely the fully nonlinear problem.

3.2.3. *Intercomparison between P_2 Solutions*

The P_2 solution with the T_7-grid is displayed on Fig. 8c. It gives an evidently bad representation of the sea-level elevation on the shelf part of the domain. Moreover, in the deep ocean, the solution appears remarkably bad though the maximum mesh size is 1/15th of the wavelength. This clearly illustrates the influence of the nonlinear damping shelf effects on the deep ocean solution.

The results of the "T_8–P_2" experiment are presented in Fig. 8d. In the deep ocean, the solution is very similar to S. But this is not quite true for the shallow areas of the domain. The sea-surface elevation results for the "T_8–P_2" test are smaller than those of the S-solution. For instance, a deficit of 30 cm can be observed along the eastern coast (for exact amplitude of 3.30 m). As far as phases are concerned, a systematic phase lag varying from 3 to 4 degrees is found between the two solutions compared here.

Figure 9 allows a more quantitative comparison. This plot reproduces a zonal section of the domain at latitude 50°, for the two solutions concerned. The westward shelf part of the channel ends at about longitude 5.5°; in that subdomain, the difference between the two solutions for the sea-surface elevation varies from

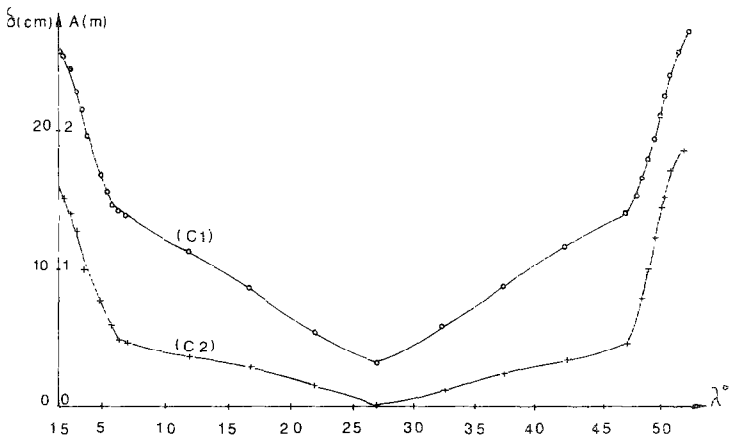

FIG. 9. Zonal section at 50°, for "$T_8 - P_2$" and S-solution comparison: (C_1) amplitude of the S-solution in m; (C_2) δ = amplitude (S-solution)—amplitude (T_8–P_2 solution) (in cm).

4.5% to 6% of the S-solution. In a transition zone, this difference is between 3.5% and 4.5%, and it is less than 3.5% in the deep ocean. Several zonal sections show exactly the same behavior of the solutions so that it can be generalized for the whole domain.

All these relative discrepancies are small; however, they are significant. If a precision of the order of some centimeters is expected for ocean tide modelling, which is the case now for satellite altimetry applications, the use of adapted grids over continental shelves is necessary to provide improved solutions over all the studied areas. Of course, over the continental shelves, nonlinear effects have to be taken into account, through the perturbation method included in formulation (1).

4. Conclusions

From the applications realized on the basis of the two analytical solutions formulated to test the precision of the finite element model developed for ocean tide computations, several rules for practical use have been clearly demonstrated:

—the necessity of adapted meshes, related to the wavelength of the modelled phenomenon, with a mean mesh size varying with the local depth of the studied areas ($\Lambda = 2\pi\omega^{-1}(gH)^{1/2}$): $\Delta L = \Lambda/15$. A precision of 10^{-3} on the elevations and 10^{-2} on the velocities can be expected for the numerical integration of the problem as formulated in (1).

—the superiority of the P_2-approximation based on economic considerations and quality criteria for the computed solutions.

—the interest of numerical integration exact only to the order 3 for P_2-approximation.

With these schematic applications and the more complex nonlinear case presented in the third part of the present work, we have illustrated the level of precision which can be expected with a correct use of that finite element model (some centimeters or less over oceanic and even continental shelf areas), and the typical errors induced by a violation of the rules formulated above. These errors can be very large over the shallow water areas where the lack of resolution is crucial, but it is important to underline that they also induce significant discrepancies in the ocean parts of the domains investigated.

All these elements will clearly be helpful for future use of that present model in practical application to the computation of real ocean tides.

Acknowledgments

This work has been supported by the Centre National de la Recherche Scientifique, the Institut Francais pour l'Exploitation de la Mer, and the Centre National d'Etudes Spatiales.

REFERENCES

1. Y. ACCAD AND C. L. PEKERIS, *Philos. Trans. Roy. Soc. London Ser. A* **290**, 235 (1978).
2. R. ARCANGELI AND J. L. GOUT, *RAIRO Anal. Numer.* **10**, 5 (1976).
3. J. J. CONNOR AND J. D. WANG, "Finite Element Modeling of Hydrodynamic Circulations," *Numerical Methods Fluid Dynamics* (Pentech, London, 1974).
4. R. ESTES, Contract NAS5-20045, Business and Technol. Systems TR-77-41, Greenbelt, Md., 1977 (unpublished).
5. G. GROTKOP, *Comput. Methods Appl. Mech. Eng.* **2**, 147 (1973).
6. V. Y. GOTLIB AND B. A. KAGAN, *D. Hydrog. Z.* **35**, 45 (1982).
7. P. C. HAMON, O. P. MARLOW, AND A. H. STROUD, *Math. Tables Aids Comput.* **10**, 130 (1956).
8. M. C. HENDERSHOTT, Geophys. *J. Roy. Astronom. Soc.* **29**, 380, (1972).
9. M. KAWAHARA AND K. HASEGAWA, *Int. J. Numer. Methods Eng.* **12**, 115 (1978).
10. J. KROHN, *Marine Geophys. Res.* **7**, 231 (1984).
11. P. H. LEBLOND AND L. A. MYSAK, *Waves in the Ocean* (Elsevier Sci. Amsterdam, 1975), p. 211.
12. C. LE PROVOST AND A. PONCET, *C R. Acad. Sci. B* **285**, 349, (1977).
13. C. LE PROVOST AND A. PONCET, *Int. J. Methods Eng.* **853**, (1978).
14. C. LE PROVOST, G. ROUGIER, AND A. PONCET, *J. Phys. Oceanogr.* **11**, No. 8, 1124 (1981).
15. D. R. LYNCH AND W. G. GRAY, *Comput. Fluids* **7**. 3 (1979).
16. D. R. LYNCH, *Oceans 81*, Vol. 2 (IEEE, New York, 1981), p. 810.
17. R. A. NICHOLAIDES, *SIAM J. Numer. Anal.* **9**. No. 3 (1972).
18. M. PARKE AND M. C. HENDERSHOTT, *Mar. Geodesy* **3**, 379 (1980).
19. M. PARKE, *Mar. Geodesy* **6**, 35 (1982).
20. C. E. PEARSON AND D. F. WINTER, *J. Phys. Oceanogr.* **7**, 520 (1977).
20. C. E. PEARSON AND D. F. WINTER, *J. Phys. Oceanogr.* 7, 520 (1977).
21. A. PONCET, Thesis, Grenoble (unpublished).
22. E. SCHWIDERSKI, Rep. NSWC/DL TR 3866, NSWC Dahlgren, Virginia, 1978 (unpublished).
23. C. TAYLOR AND J. M. DAVIES, *Finite Elements in Fluids* (Wiley, 1975).
24. W. ZAHEL, *Ann. Geophys.* **T.33**, fasc 1/2, 31 (1977).